Thermal simulations and measurements of 3-phase medium frequency transformer in 100 kW DC-DC converter with 99.2% efficiency

Piotr Dworakowski, Michal Michna, Andrzej Wilk

Thermal simulations and measurements of 3-phase medium frequency transformer in 100 kW DC-DC converter with 99.2% efficiency

Piotr Dworakowski, Michał Michna*, Andrzej Wilk*

SuperGrid Institute, Villeurbanne, France
piotr.dworakowski@supergrid-institute.com

* Gdansk University of Technology, Faculty of Electrical and Control Engineering, Gdańsk, Poland
michal.michna@pg.edu.pl, andrzej.wilk@pg.edu.pl

***Abstract* - This article deals with a 100 kW dual active bridge (DAB) DC-DC converter and a 20 kHz 3-phase medium frequency transformer (MFT). A computational fluid dynamics (CFD) model of the MFT is presented and compared with thermal measurements showing a good fit. The core hotspot is close to the thermal runaway limit. The maximum winding temperature in the normal operating mode results in a comfortable headroom to enable the operation in the degraded mode. Moreover, it is likely that the transformer may be loaded with higher power. The efficiency of the DC-DC converter was measured 99.2% at 100 kW.**

I. INTRODUCTION

The isolated DC-DC converter is the enabling technology in modern electrical power systems and transportation [1]. Dual active bridge (DAB) is a prominent topology for high power applications requiring bidirectional power flow [2]. The 3-phase DAB (DAB3) is considered for the applications where high power density and high efficiency are required [3], [4].

A medium frequency transformer (MFT) is one of the key components of the isolated DC-DC converters. The MFT is still quite a novel technology with lots of research interest [5]–[8]. In particular, only a few 3-phase MFT have been reported. A 10 kVA 1 kHz 3-phase MFT prototype was reported in [9] and a 2 kVA 100 kHz 3-phase MFT was reported in [10]. A 5 MW DAB3 was presented in [11] but using three single-phase MFTs. The 3-phase MFT at high power (100 kW) and high frequency (20 kHz) was reported by the authors in [12]. The design of MFT must consider winding, core, insulation and cooling design constraints.

The choice of magnetic core material shall be done according to the material properties and cost [13], [14]. The amorphous and especially nanocrystalline materials are preferred in low and medium frequencies due to the high flux density. The main advantage of ferrite cores is their low power loss, which makes them an attractive material for the construction of medium and high frequency transformers [15], [16]. The magnetic circuit can be realised with different geometrical structures: core type [17], shell type [18], matrix [19] or coaxial [20].

The design of MFT winding must take into account the skin and proximity effects. The foil winding is the cheapest but it causes a large parasitic capacitance of the winding [21]. The tube conductor requires a specific manufacturing process and results with the significant conductor diameter [22]. The litz wire offers a good performance but it comes with a relatively high cost.

The insulation of MFT may be ensured by solid or liquid material. The solid insulation offers the dielectric strength of some tens of kV/mm. Usually it is realised by the impregnation of a material placed between the windings. In case of a breakdown the insulation material is definitively damaged. The advantage of the solid insulation is a limited maintenance. The liquid insulation, in addition to its primary function offers good cooling. A liquid-insulated transformer would be generally smaller than a solid-insulated one. However, the liquid insulation requires more maintenance effort and depending on the liquid used it may be more or less environmentally friendly. In MFT design, the high frequency effect on insulation material should be taken into account [23], [24].

The cooling of the MFT may be ensured by the natural or forced air convection or liquid cooling [25]. The liquid cooling offers the best performance but it requires more complex cooling system and more important maintenance effort. The liquid cooling may be considered if a very high-power density is required or if the liquid is required for insulation. The thermal design of MFT is challenging due to the high-power loss density of a small size MFT.

There is a research competition in designing the highest efficiency DC-DC converter and MFT while keeping the small size. Mastering the power losses and simple cooling is the key to the successful design. This article presents the thermal design and efficiency measurement of a 3-phase MFT within a 100 kW DAB DC-DC converter. The measured efficiency of the isolated DC-DC converter is 99.2%.

This article is organised as follows. Section II introduces the 3-phase DAB DC-DC converter and the MFT. Section III presents a computational fluid dynamics (CFD) model of the MFT. Section IV details the thermal measurements of the MFT including a comparison with the CFD simulation. Section V shows the efficiency measurement of the 100 kW DC-DC converter.

II. 3-PHASE DAB AND MFT

The 3-phase DAB (DAB3) is composed of two 3-phase bridges connected with a 3-phase transformer. The DAB3 circuit diagram is presented in Fig. 1. The operation of the DAB3 with the rectangular modulation is based on the phase shift δ between two bridges. The power flow is inversely proportional to the MFT leakage inductance L_{ac}. A 100 kW DC-DC converter prototype was developed as detailed in [26]. Both bridges are equipped with 1.7 kV SiC MOSFET [27]. The normal operation mode is defined as $U_{dc1} = U_{dc2} = 1200$ V and the degraded operation mode as $U_{dc1} = 1200$ V and $U_{dc2} = 0.8U_{dc1}$.

The design of the 3-phase MFT was detailed by the authors in [12]. The main data are summarized in Table I. The winding losses were calculated according to [28], which is derived from

[29]. The core losses were calculated according to [30], which is derived from [31].

The 3-phase MFT power density is approximately 4 kVA/kg. A comparable 50 Hz transformer, at 400 V and natural air cooling, has the power density of less than 0.4 kVA/kg [32]. The 3-phase MFT at 20 kHz is more than 10 times lighter than the 3-phase 50 Hz transformer.

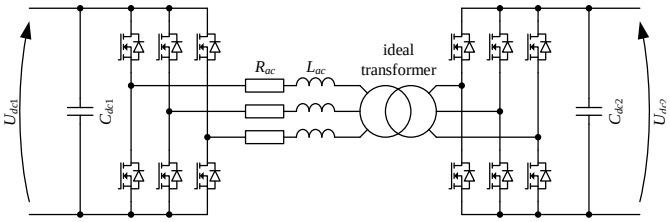

Fig. 1. Circuit model of the 3-phase dual active bridge (DAB3)

TABLE I
3-PHASE MFT DATASHEET

Rated active power	100 kW
Primary and secondary phase voltage	566 V RMS
Primary and secondary current (normal/degraded)	65 / 92 A RMS
Frequency	20 kHz
Vector group and core structure	Yy core type
Winding material	copper litz wire
Number of turns	20 (single layer)
Winding wire cross section	30.39 mm^2
Winding current density (normal/degraded)	2.1 / 3 A/mm^2
Winding wire strand diameter	0.1 mm
Number of strands	3870
Winding wire packing factor	0.56
Winding equivalent resistance at 60°C (normal/degraded) R_{ac}	16.5 / 13.6 mΩ
Calculated winding power loss at 60°C (normal/degraded)	206 / 347 W
Leakage inductance L_{ac}	16 µH
Magnetizing inductance (approx. value)	1 mH
Primary winding capacitance (approx. value)	65 pF
Secondary winding capacitance (approx. value)	60 pF
Primary-secondary capacitance	80 pF
Core material	ferrite 3C90 I-core
Core cross-section	12.5 cm^2
Maximum flux density	0.27 T
Calculated core power loss at 120°C	255 W
Insulation voltage	5 kV
Insulation class	H
Cooling	forced air
Weight	36 kg

III. CFD SIMULATION MODEL OF MFT

A computational fluid dynamics (CFD) model of the 3-phase MFT was developed in Ansys Icepak. Ansys Icepak is based on the Fluent solver which solves Navier-Stokes equations. The equation for conservation of mass can be written as follows:

$$\frac{\partial \rho}{\partial t} + \nabla \cdot (\rho \mathbf{v}) = 0\,, \tag{1}$$

where $\rho(\mathbf{x},t)$ is the fluid density which is a function of time t and position vector $\mathbf{x}$ and $\mathbf{v}$ is the fluid velocity vector. For an incompressible fluid (1) reduces to:

$$\nabla \cdot \mathbf{v} = 0 \tag{2}$$

The law of conservation of momentum is:

$$\rho \frac{\partial (\rho \mathbf{v})}{\partial t} + \nabla \cdot (\rho \mathbf{v}\mathbf{v}) = -\nabla p + \nabla \cdot \boldsymbol{\tau} + \rho \mathbf{g} + \mathbf{F}\,, \tag{3}$$

where p is the static pressure, $\boldsymbol{\tau}$ is the stress tensor, $\mathbf{g}$ is the standard gravity vector and $\mathbf{F}$ is the external force vector. The stress tensor describes the momentum transfer on the surface of the fluid. For the Newtonian fluid, the stress tensor is proportional to the velocity gradient tensor:

$$\boldsymbol{\tau} = \mu \left[\nabla \mathbf{v} + \nabla \mathbf{v}^{\mathbf{T}} - \frac{2}{3} \nabla \mathbf{v} \mathbf{I} \right], \tag{4}$$

where μ is the molecular viscosity, $\mathbf{I}$ is the unit tensor. The energy equation considers the flow of mass and heat:

$$\frac{\partial}{\partial t}(\rho h) + \nabla \cdot (\rho h \mathbf{v}) = \nabla \cdot [(k + k_t)\nabla T] + S_h\,, \tag{5}$$

where h is the sensible enthalpy, k he molecular conductivity, k_t is the conductivity due to turbulent transport, T is the temperature, S_h includes any volumetric heat sources. In conducting solid regions, Ansys Icepak solves a simple conduction equation that includes the heat flux due to conduction and volumetric heat sources within the solid:

$$\frac{\partial}{\partial t}(\rho h) = \nabla \cdot [k \nabla T] + S_h \tag{6}$$

The 3D model of the MFT presented in Fig. 2 was divided into four computational domains and the material properties were set as follows:

- Ω_1 is the homogenized ferrite core with the thermal conductivity λ = 4.25 W/mK, specific heat c = 750 J/kgK, density ρ = 4800 kg/m^3 [33],
- Ω_2 is the litz wire winding; in [34] a thermal model of a litz wire was proposed showing that the transverse thermal conductivity is below 1 W/mK; in the Icepak library, the material which has similar properties is epoxy resin with λ = 0.2 W/mK; hence, this homogenized material was used,
- Ω_3 is the background region with the air temperature 40°C,
- Ω_4 is the volume of fans with the same material properties as Ω_3.

The emissivity coefficient of the core and winding was set to ε = 0.8. A turbulent air flow was considered. The bottom face of the background region is a wall with zero heat flux and all other faces are openings with constant temperature at 40°C.

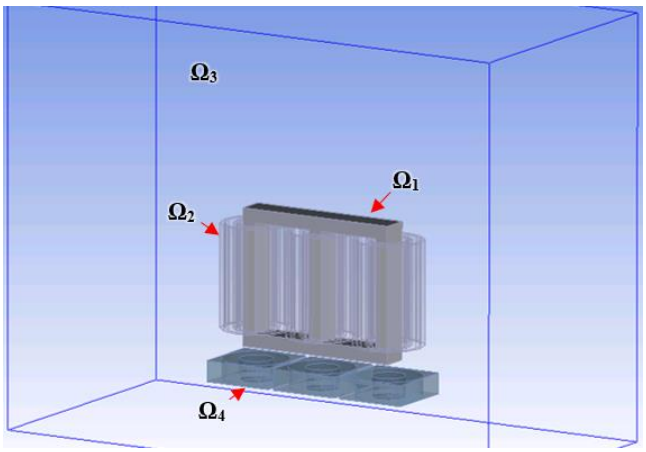

Fig. 2. CFD model of MFT including the domains: Ω_1 core, Ω_2 winding, Ω_3 background and Ω_4 fans

Three fans EBM papst 5214 NHH [35] were implemented with the linearized pressure-flow curve as presented in Fig. 3.

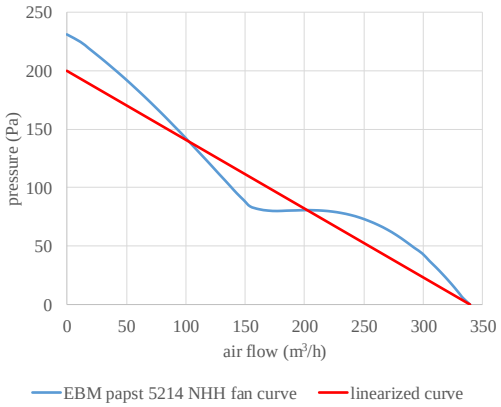

Fig. 3. EBM papst 5214 NHH fan curve [35] (blue) and linearized curve for CFD simulation (red)

The heat sources were assigned according to the winding and core power loss presented in Table I for the normal operating mode. The simulation result is presented in Fig. 4 showing the air velocity vectors displayed on a side view plane passing vertically across the middle of transformer and in Fig. 9 showing the temperature distribution on the core surface. It is seen that the windings are well cooled thanks to the air passing between the windings. The core is not cooled so well.

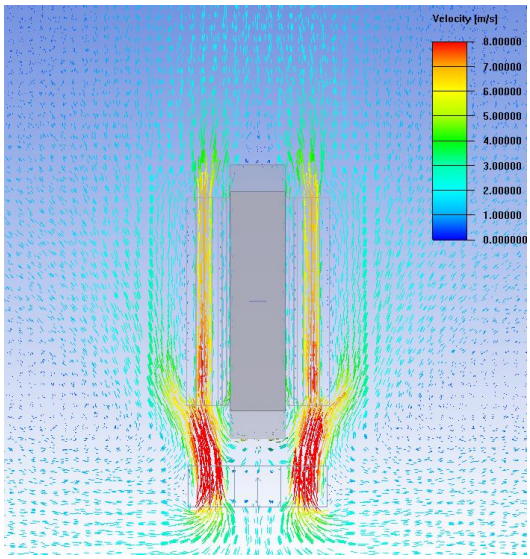

Fig. 4. Thermal simulation result in steady state showing the air velocity vectors on a plane passing vertically across the middle of transformer, side view

IV. THERMAL TEST OF MFT

A. Test bench

A dedicated power converter test bench was developed allowing the experimental validation of the 3-phase DAB and MFT. The circuit diagram is presented in Fig. 5 and the test bench implementation in Fig. 6. The power circuit is arranged in back-to-back in order to test the DC-DC converter at full power with minimum energy consumption. The converter output is connected to its input and the whole is supplied from a DC power supply which sets the voltage reference and supplies the test circuit power loss. The DC-DC converter runs in the power regulation mode. The current transducers in the AC link are necessary for the internal converter protection and the control of DC bias [36].

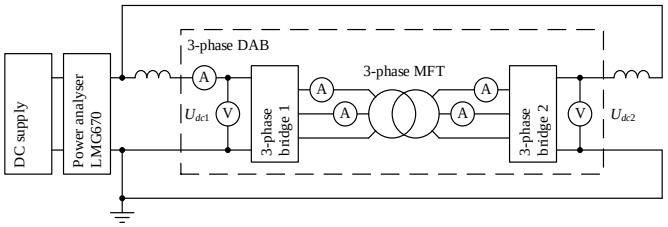

Fig. 5. Circuit diagram of the test bench with 3-phase DAB DC-DC converter

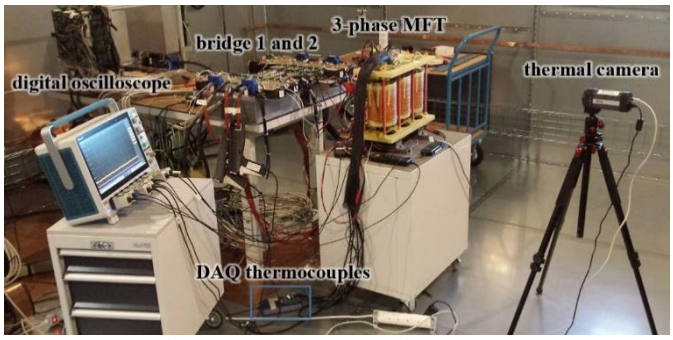

Fig. 6. Test bench for thermal measurements of the 100 kW DC-DC converter

B. Thermal test

The thermal test was performed at $U_{dc1} = U_{dc2} = 1200$ V and 100 kW corresponding to the normal operating mode. The MFT temperature was measured with some thermocouples placed around the transformer during the manufacturing. An additional measurement was done using a thermal camera. In Fig. 7 the thermal test result is presented showing the values of temperature rise ΔT. The test lasted for 6 hours. Some disturbances are present in the waveforms due to unintentional converter stops related to gate-drive EMI problems [37], [38]. At the end of the record the temperatures were stabilized and it seems fair to consider them as final values. The ambient temperature varied during the test between 23 and 37°C. At the end of the test the ambient temperature was close to 40°C set in CFD simulation.

As expected, the temperature of the central column (measured by thermocouples Tc2, Tc3, Tc4) is the highest, with Tc3 being the hotspot equal to 127°C (ΔT = 90 K). The core temperature is probably close to the thermal runaway limit. The Curie temperature of 3C90 is 220°C. The time constant of the hotspot is approximately 0.6 hours. The temperature of the side column (Tc10) is equal to 93°C.

The primary winding temperature (Tc5) is 56°C and the secondary winding temperature (Tc6) is nearly the same as ambient. The temperature of the insulation class H is respected. Some temperature margin is required to enable the DC-DC converter operation in degraded mode where the winding power loss is almost doubled when compared to the normal operation mode. Moreover, it is likely that the transformer may be loaded with higher power.

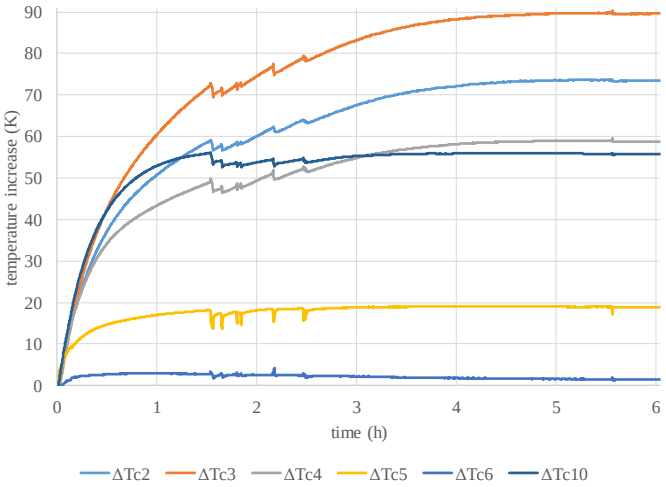

Fig. 7. Thermal test result of the 3-phase MFT: core (Tc2, Tc3, Tc4 and Tc10) and winding (Tc5 and Tc6) temperature increase ΔT at the ambient temperature of 37°C maximum

In Fig. 8 there is presented the measured temperature distribution on the MFT surface using the thermal camera Flir A325 [39]. The values should be considered approximate as the default thermal camera emissivity coefficients where used. The temperature measurement could be more precise if the emissivity coefficients were set. The general trend of temperature distribution is confirmed. The core central column is the hottest. The core yoke is cooler than the core side columns thanks to better heat exchange. The external winding is nearly at the ambient temperature.

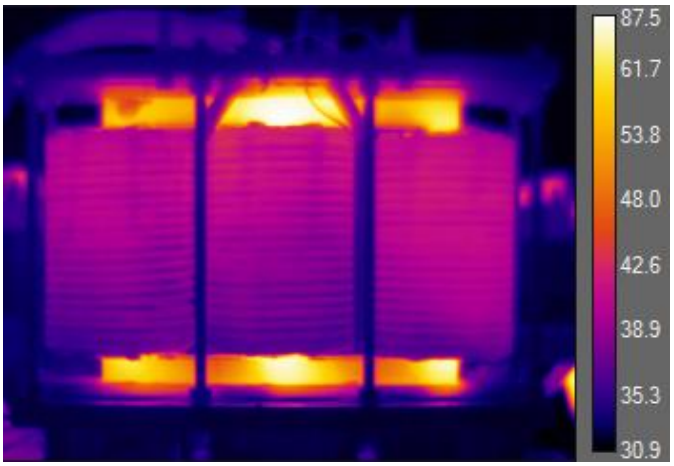

Fig. 8. Thermal image of the 3-phase MFT

C. Comparison between simulation and experimental results

In Fig. 9 there is presented the comparison between the CFD simulation and measurement. The temperature on the core surface is plotted and the values at the thermocouple locations are displayed. The red text gives the simulation result and the black text gives the measurement result. The measured temperature of the side column at 93°C is very similar to the simulated value at 90°C. The temperature of the central column is quite similar to the surface hotspot temperature simulated at 120°C and measured at around 127°C. The distribution of the temperature along the column height is not the same. The simulation indicates the hotspot localisation in the 2/3 of the column height whereas the measurement indicates it in the column centre.

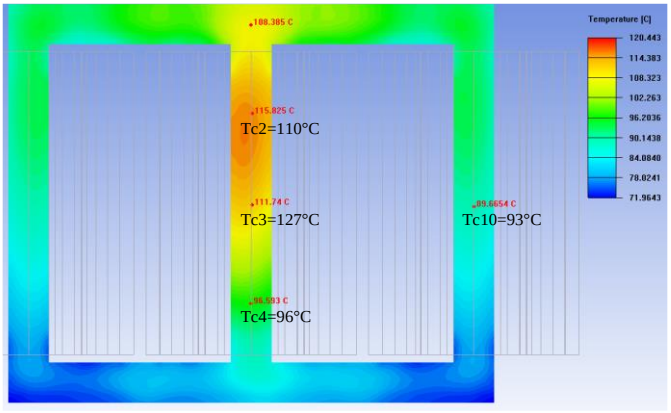

Fig. 9. Comparison between the thermal simulation (surface plot) and thermal measurement (text in black)

V. EFFICIENCY MEASUREMENT OF DC-DC CONVERTER

The measurement of the DC-DC converter efficiency was performed using the precision power analyser ZES Zimmer LMG670 [40]. The power of the DC supply was measured according to Fig. 6. This measurement technique was proven to be the most effective and rather overestimating the DC-DC converter power loss. This measurement takes into account the power loss of the complete test bench, including the DC-DC converter but also DC inductors and all wiring. The authors highlight that the measurement of power losses in highly efficient power converters is a metrological challenge. In this article, the DC-DC converter efficiency was measured accurately thanks to the converter ratio equal to 1.

The efficiency measurement result is presented in Fig. 10. At $U_{dc1} = U_{dc2} = 1200$ V and 100 kW, the DC-DC efficiency is 99.2%. A maximum efficiency of 99.25% is seen at 70 kW. Considering the transformer power loss contribution, the shape of the curve is as expected. Low efficiency at low power is due to the loss of zero voltage switching (ZVS) [41], [42].

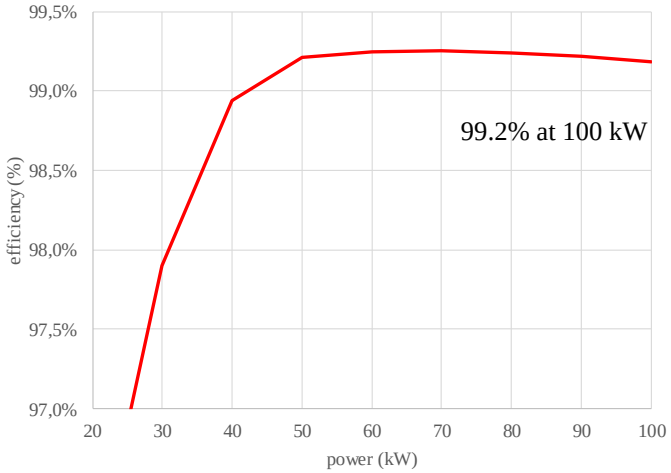

Fig. 10. Efficiency measurement of the 3-phase DAB. At 100 kW the DC-DC efficiency is 99.2%. Low efficiency at low power is due to the loss of zero voltage switching (ZVS)

Assuming that the half of the power loss accounts for MFT then the half for the SiC MOSFETs [43], the 3-phase MFT efficiency is expected approximately 99.6%. This corresponds to the MFT power loss at 400 W what is slightly lower than calculated in Table I (206+255=461 W). This is in line with the investigations presented in [44] where a new set of Steinmetz equation coefficients was proposed. However, if the power loss calculations are not valid, then it is surprising to see the good fit between the thermal simulation and measurements presented in section IV. Further analysis is required. In order to measure the MFT efficiency, the calorimetric methods should be considered [45]. The measurement of MFT efficiency using ZES Zimmer LMG670 was not successful.

VI. CONCLUSION

The 100 kW dual active bridge (DAB) converter and the 20 kHz 3-phase medium frequency transformer (MFT) were presented. The computational fluid dynamics (CFD) model of the 3-phase MFT was introduced. The thermal measurements of the MFT were detailed and compared with the CFD simulation. The efficiency of the DC-DC converter was measured.

The CFD simulation and experimental measurements show a good fit. The MFT surface hotspot is in the central column at 127°C. This high temperature is probably close to the thermal runaway limit but still well below the Curie temperature at 220°C. The maximum winding temperature in the normal operating mode is at the comfortable 56°C. There is enough headroom to enable the operation in degraded mode where the winding power loss is almost doubled. Moreover, it is likely that the transformer may be loaded with higher power.

The efficiency of the DC-DC converter was measured 99.2% at 100 kW. This is an accurate measurement which was only possible thanks to the DC-DC conversion ratio equal to 1. The 3-phase MFT efficiency is expected at approximately 99.6%. Any direct MFT efficiency measurement was not successful. Further research is required in order to identify an appropriate efficiency measurement method for MFT.

REFERENCES

[1] P. Dworakowski, "Modelling and analysis of medium frequency transformers for power converters," PhD thesis, Gdansk University of Technology, 2020.

[2] R. W. A. A. De Doncker, D. M. Divan, and M. H. Kheraluwala, "A three-phase soft-switched high-power-density DC/DC converter for high-power applications," *IEEE Transactions on Industry Applications*, vol. 27, no. 1, pp. 63–73, Jan. 1991.

[3] N. Soltau, H. Stagge, R. W. De Doncker, and O. Apeldoorn, "Development and demonstration of a medium-voltage high-power DC-DC converter for DC distribution systems," in *2014 IEEE 5th International Symposium on Power Electronics for Distributed Generation Systems (PEDG)*, 2014, pp. 1–8.

[4] J. Xue, F. Wang, D. Boroyevich, and Z. Shen, "Single-phase vs. three-phase high density power transformers," in *2010 IEEE Energy Conversion Congress and Exposition*, 2010, pp. 4368–4375.

[5] M. Mogorovic and D. Dujic, "100 kW, 10 kHz Medium-Frequency Transformer Design Optimization and Experimental Verification," *IEEE Transactions on Power Electronics*, vol. 34, no. 2, pp. 1696–1708, Feb. 2019.

[6] I. Villar, L. Mir, I. Etxeberria-Otadui, J. Colmenero, X. Agirre, and T. Nieva, "Optimal design and experimental validation of a Medium-Frequency 400kVA power transformer for railway traction applications," in *2012 IEEE Energy Conversion Congress and Exposition (ECCE)*, 2012, pp. 684–690.

[7] G. Ortiz, J. Biela, D. Bortis, and J. W. Kolar, "1 Megawatt, 20 kHz, isolated, bidirectional 12kV to 1.2kV DC-DC converter for renewable energy applications," in *The 2010 International Power Electronics Conference - ECCE ASIA -*, 2010, pp. 3212–3219.

[8] B. Z. Tomczuk, D. Koteras, and A. Waindok, "Electromagnetic and Temperature 3-D Fields for the Modular Transformers Heating Under High-Frequency Operation," *IEEE Transactions on Magnetics*, vol. 50, no. 2, pp. 317–320, Feb. 2014.

[9] Y. Lee, G. Vakil, Alan. J. Watson, and P. W. Wheeler, "Geometry optimization and characterization of three-phase medium frequency transformer for 10kVA Isolated DC-DC converter," in *2017 IEEE Energy Conversion Congress and Exposition (ECCE)*, 2017, pp. 511–518.

[10] M. Noah *et al.*, "A novel three-phase LLC resonant converter with integrated magnetics for lower turn-off losses and higher power density," in *2017 IEEE Applied Power Electronics Conference and Exposition (APEC)*, 2017, pp. 322–329.

[11] N. Soltau, H. Stagge, R. W. De Doncker, and O. Apeldoorn, "Development and demonstration of a medium-voltage high-power DC-DC converter for DC distribution systems," in *2014 IEEE 5th International Symposium on Power Electronics for Distributed Generation Systems (PEDG)*, 2014, pp. 1–8.

[12] P. Dworakowski, A. Wilk, M. Michna, B. Lefebvre, and T. Lagier, "3-phase medium frequency transformer for a 100kW 1.2kV 20kHz Dual Active Bridge converter," in *IECON 2019 - 45th Annual Conference of the IEEE Industrial Electronics Society*, 2019, vol. 1, pp. 4071–4076.

[13] I. Villar, A. Garcia-Bediaga, U. Viscarret, I. Etxeberria-Otadui, and A. Rufer, "Proposal and validation of medium-frequency power transformer design methodology," in *2011 IEEE Energy Conversion Congress and Exposition*, 2011, pp. 3792–3799.

[14] W. G. Hurley, T. Merkin, and M. Duffy, "The Performance Factor for Magnetic Materials Revisited: The Effect of Core Losses on the Selection of Core Size in Transformers," *IEEE Power Electronics Magazine*, vol. 5, no. 3, pp. 26–34, Sep. 2018.

[15] M. A. Bahmani, "Design considerations of medium-frequency power transformers in HVDC applications," in *2017 Twelfth International Conference on Ecological Vehicles and Renewable Energies (EVER)*, 2017, pp. 1–6.

[16] M. Stojadinović and J. Biela, "Modelling and Design of a Medium Frequency Transformer for High Power DC-DC Converters," in *2018 International Power Electronics Conference (IPEC-Niigata 2018 - ECCE Asia)*, 2018, pp. 1103–1110.

[17] I. Villar, L. Mir, I. Etxeberria-Otadui, J. Colmenero, X. Agirre, and T. Nieva, "Optimal design and experimental validation of a Medium-Frequency 400kVA power transformer for railway traction applications," in *2012 IEEE Energy Conversion Congress and Exposition (ECCE)*, 2012, pp. 684–690.

[18] M. Mogorovic and D. Dujic, "100 kW, 10 kHz Medium-Frequency Transformer Design Optimization and Experimental Verification," *IEEE Transactions on Power Electronics*, vol. 34, no. 2, pp. 1696–1708, Feb. 2019.

[19] G. Ortiz, J. Biela, D. Bortis, and J. W. Kolar, "1 Megawatt, 20 kHz, isolated, bidirectional 12kV to 1.2kV DC-DC converter for renewable energy applications," in *The 2010 International Power Electronics Conference - ECCE ASIA -*, 2010, pp. 3212–3219.

[20] M. H. Kheraluwala, D. W. Novotny, and D. M. Divan, "Coaxially wound transformers for high-power high-frequency applications," *IEEE Transactions on Power Electronics*, vol. 7, no. 1, pp. 54–62, Jan. 1992.

[21] P. Dworakowski, A. Wilk, and B. Lefebvre, "Hysteresis modelling of a medium frequency single-phase transformer," in *2017 19th European Conference on Power Electronics and Applications (EPE'17 ECCE Europe)*, 2017, p. P.1-P.9.

[22] L. Heinemann, "An actively cooled high power, high frequency transformer with high insulation capability," in *APEC. Seventeenth Annual IEEE Applied Power Electronics Conference and Exposition (Cat. No.02CH37335)*, 2002, vol. 1, pp. 352–357 vol.1.

[23] M. Birle and C. Leu, "Breakdown of polymer dielectrics at high direct and alternating voltages superimposed by high frequency high voltages," in *2013 IEEE International Conference on Solid Dielectrics (ICSD)*, 2013, pp. 656–661.

[24] S. Anand, E. Vagnon, A. Zouaghi, M. Guillet, C. Buttay, and O. Agri, "Electrical and optical partial discharge assessment of dielectric barriers

in mineral oil and synthetic ester," in *2021 IEEE Electrical Insulation Conference (EIC)*, 2021, pp. 602–605.
[25] G. Ortiz, J. Biela, and J. W. Kolar, "Optimized design of medium frequency transformers with high isolation requirements," in *IECON 2010 - 36th Annual Conference on IEEE Industrial Electronics Society*, 2010, pp. 631–638.
[26] T. Lagier *et al.*, "A 100 kW 1.2 kV 20 kHz DC-DC converter prototype based on the Dual Active Bridge topology," in *2018 IEEE International Conference on Industrial Technology (ICIT)*, 2018, pp. 559–564.
[27] Wolfspeed, "CAS300M17BM2 1700V 225A 8.0mΩ SiC Half-Bridge." [Online]. Available: https://www.wolfspeed.com/power/products/sic-power-modules/cas300m17bm2. [Accessed: 01-Jan-2020].
[28] F. Tourkhani and P. Viarouge, "Accurate analytical model of winding losses in round Litz wire windings," *IEEE Transactions on Magnetics*, vol. 37, no. 1, pp. 538–543, Jan. 2001.
[29] P. L. Dowell, "Effects of eddy currents in transformer windings," *Proceedings of the Institution of Electrical Engineers*, vol. 113, no. 8, pp. 1387–1394, Aug. 1966.
[30] K. Venkatachalam, C. R. Sullivan, T. Abdallah, and H. Tacca, "Accurate prediction of ferrite core loss with nonsinusoidal waveforms using only Steinmetz parameters," in *2002 IEEE Workshop on Computers in Power Electronics, 2002. Proceedings.*, 2002, pp. 36–41.
[31] Chas. P. Steinmetz, "On the Law of Hysteresis," *Transactions of the American Institute of Electrical Engineers*, vol. IX, no. 1, pp. 1–64, Jan. 1892.
[32] ABB, "Dry-type low voltage transformers," 2014. [Online]. Available: https://search-ext.abb.com/library/Download.aspx?DocumentID=1LES100025-ZD&LanguageCode=en&DocumentPartId=&Action=Launch. [Accessed: 12-Jan-2020].
[33] Ferroxcube, "Soft ferrites and accessories, data handbook," 2013. [Online]. Available: https://www.ferroxcube.com/en-global/download/download/11. [Accessed: 01-Jan-2020].
[34] P. A. Kyaw, J. Qiu, and C. R. Sullivan, "Analytical Thermal Model for Inductor and Transformer Windings and Litz Wire," in *2018 IEEE 19th Workshop on Control and Modeling for Power Electronics (COMPEL)*, 2018, pp. 1–9.
[35] ebm-papst, "DC axial compact fan 5214 NHH." [Online]. Available: https://img.ebmpapst.com/products/datasheets/DC-axial-fan-5214NHH-ENU.pdf?_ga=2.136622008.944340178.1582828446-718160680.1582828446. [Accessed: 27-Feb-2020].
[36] M. Wattenberg, U. Schwalbe, and M. Pfost, "Impact of DC-Bias on Dual Active Bridge Control and How to Avoid it," in *2019 21st European Conference on Power Electronics and Applications (EPE '19 ECCE Europe)*, 2019, p. P.1-P.8.
[37] H. Geramirad *et al.*, "Experimental EMI study of a 3-phase 100kW 1200V Dual Active Bridge Converter using SiC MOSFETs," in *2020 22nd European Conference on Power Electronics and Applications (EPE'20 ECCE Europe)*, 2020, pp. 1–10.
[38] H. Geramirad *et al.*, "Conducted EMI reduction in a 100kW 1.2kV Dual Active Bridge converter," in *PCIM Europe digital days 2020; International Exhibition and Conference for Power Electronics, Intelligent Motion, Renewable Energy and Energy Management*, 2020, pp. 1–8.
[39] FLIR, "Thermal camera A325sc." [Online]. Available: https://www.flir.com/products/a325sc/. [Accessed: 22-Mar-2020].
[40] ZES Zimmer, "LMG670 - 1 to 7 Channel Power Analyzer." [Online]. Available: https://www.zes.com/en/Products/Discontinued-Products/Energy-and-Power-Meters/LMG670. [Accessed: 06-Mar-2020].
[41] T. Lagier *et al.*, "Experimental validation and comparison of a SiC MOSFET based 100 kW 1.2 kV 20 kHz three-phase dual active bridge converter using two vector groups," in *2020 22nd European Conference on Power Electronics and Applications (EPE'20 ECCE Europe)*, 2020, p. P.1-P.9.
[42] T. Lagier and P. Ladoux, "Theoretical and experimental analysis of the soft switching process for SiC MOSFETs based Dual Active Bridge converters," in *2018 International Symposium on Power Electronics, Electrical Drives, Automation and Motion (SPEEDAM)*, 2018, pp. 262–267.
[43] H. Akagi, T. Yamagishi, N. M. L. Tan, S. Kinouchi, Y. Miyazaki, and M. Koyama, "Power-loss breakdown of a 750-V, 100-kW, 20-kHz bidirectional isolated DC-DC converter using SiC-MOSFET/SBD dual modules," in *2014 International Power Electronics Conference (IPEC-Hiroshima 2014 - ECCE ASIA)*, 2014, pp. 750–757.
[44] M. Michna, P. Dworakowski, A. Wilk, F. Kutt, and M. Mermet-Guyennet, "Modified Preisach model of hysteresis in multi air gap ferrite core medium frequency transformer," *IEEE Transactions on Power Delivery*, pp. 1–1, 2021.
[45] D. Rothmund, T. Guillod, D. Bortis, and J. W. Kolar, "99% Efficient 10 kV SiC-Based 7 kV/400 V DC Transformer for Future Data Centers," *IEEE Journal of Emerging and Selected Topics in Power Electronics*, vol. 7, no. 2, pp. 753–767, Jun. 2019.